Cell, Volume *131*

Supplemental Data

Architecture of a Coat for the Nuclear Pore Membrane

Kuo-Chiang Hsia, Pete Stavropoulos, Günter Blobel, and André Hoelz

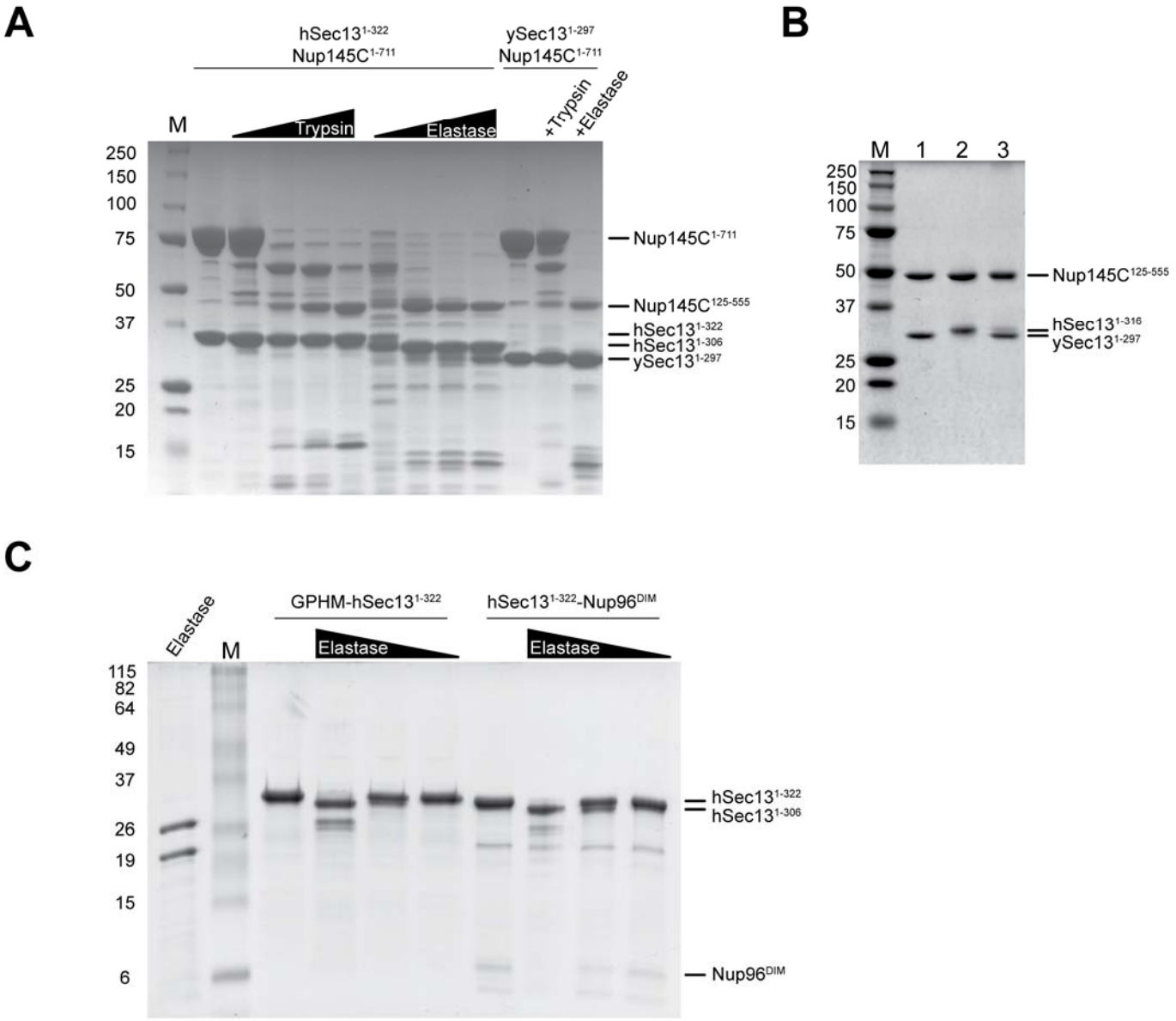

Figure S1. Characterization of the Sec13-Nup145C Complex *in Vitro* and *in Vivo.* (**A**) Limited proteolysis of full-length human Sec13-Nup145C and yeast Sec13-Nup145C complexes with various proteases. (**B**) Human Sec13 can replace its yeast homolog in the Nup145C complex when co-expressed in *E. coli*. Lane 1, yeast Sec13-Nup145C complex; lane 2, human Sec13-Nup145C complex; lane 3, human and yeast Sec13-Nup145C complex mixture. The proteins were co-purified, and the peak fractions of the gel filtration step were analyzed by SDS-PAGE and Coomassie staining. (**C**) Limited proteolysis of human Sec13 and human Sec13-Nup96^{DIM}. Coomassie-stained SDS-polyacrylamide gel, illustrating the proteolytic pattern of Sec13 and Sec13-Nup96^{DIM} using elastase. The higher molecular weight of human Sec13 in isolation results from the N-terminal overhang (GPHM) left after PreScision protease cleavage. The C-terminal Sec13 tail is accessible for proteolytic cleavage in both cases. The identity of the various fragments was determined by N-terminal protein sequencing and mass spectrometry.

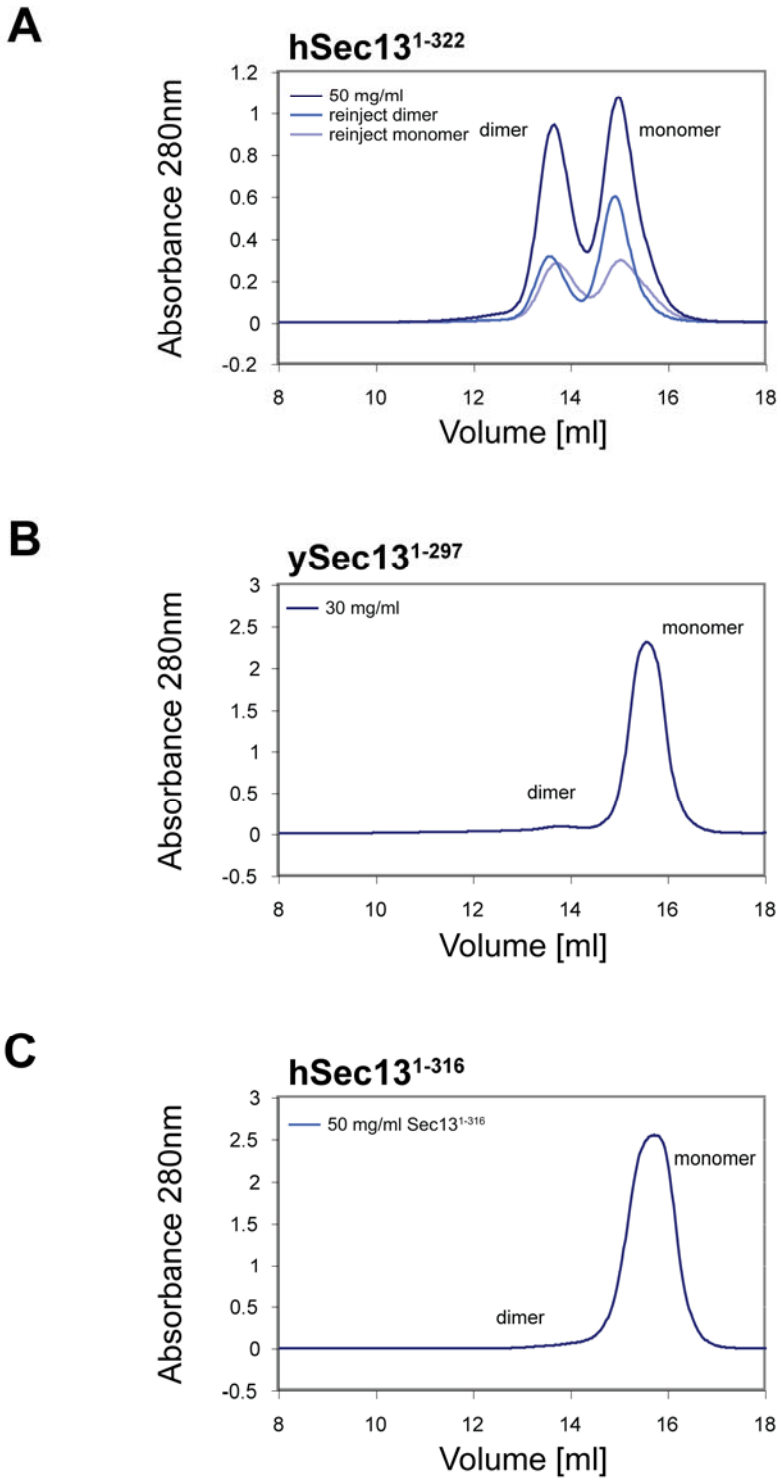

Figure S2. Analysis of Oligomeric State of Sec13 in Isolation. (**A**) Gel filtration profiles of the full-length human Sec13$^{1-322}$. The protein forms a dynamic equilibrium between monomers and dimers in solution. (**B**) Gel filtration profile of full-length yeast Sec13$^{1-297}$. This protein forms a dynamic equilibrium between monomers and dimers in solution. (**C**) Gel filtration profile of a C-terminally truncated human Sec13$^{1-316}$. This protein is mainly monomeric in solution with barely detectable amounts of dimer. All proteins were injected at the indicated concentrations.

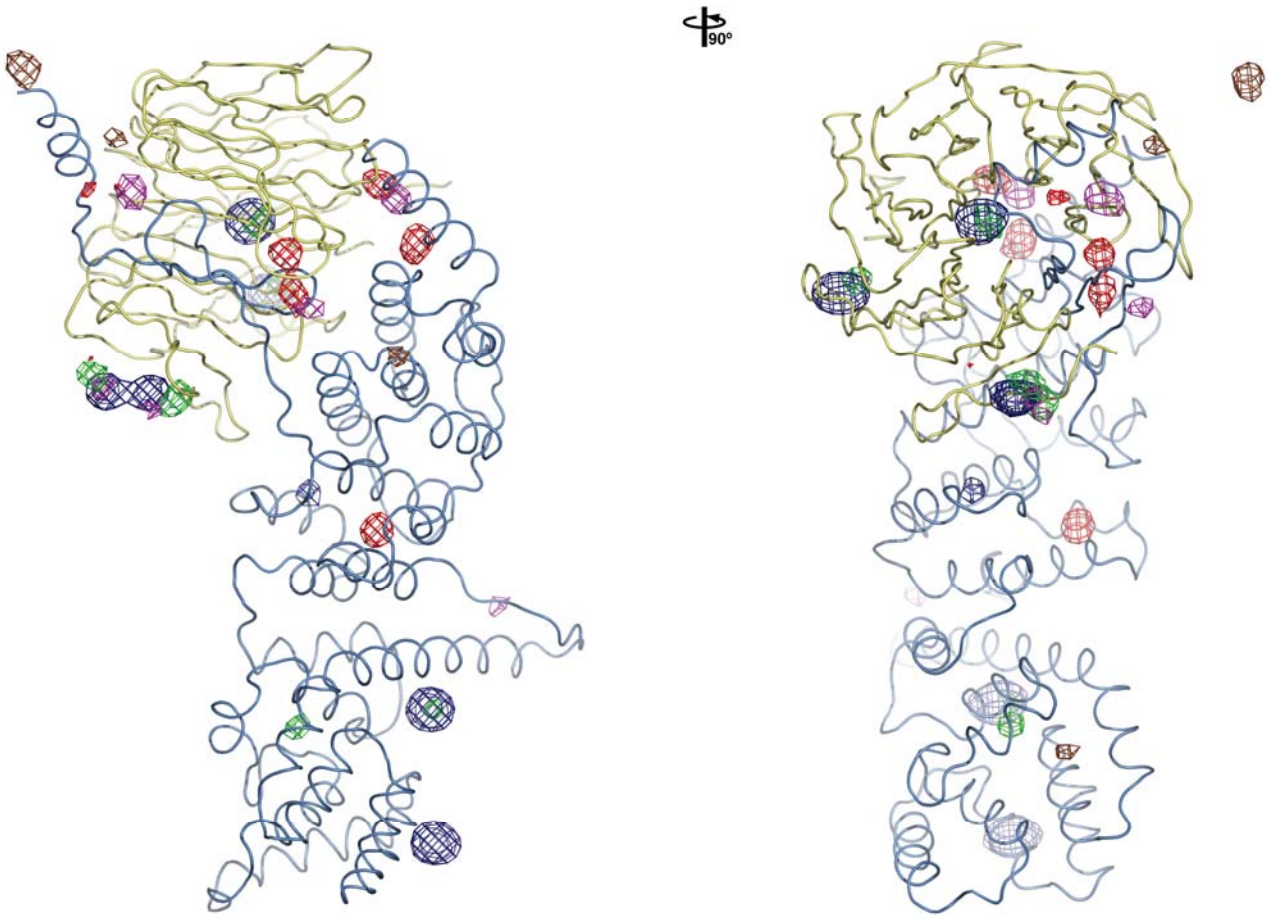

Figure S3. Experimental Phasing. Anomalous difference Fourier maps, illustrating selenium (red), osmium (blue), mercury (green), platinum (magenta), and $[Ta_6Br_{12}]^{2+}$ cluster (orange) sites, calculated from x-ray diffraction data obtained from the orthorhombic crystal form. A 90° rotated view is shown on the right. For clarity, only one of the four Sec13-Nup145C complexes in the asymmetric unit is shown. Similar results were obtained with the x-ray diffraction data of the monoclinic crystal form.

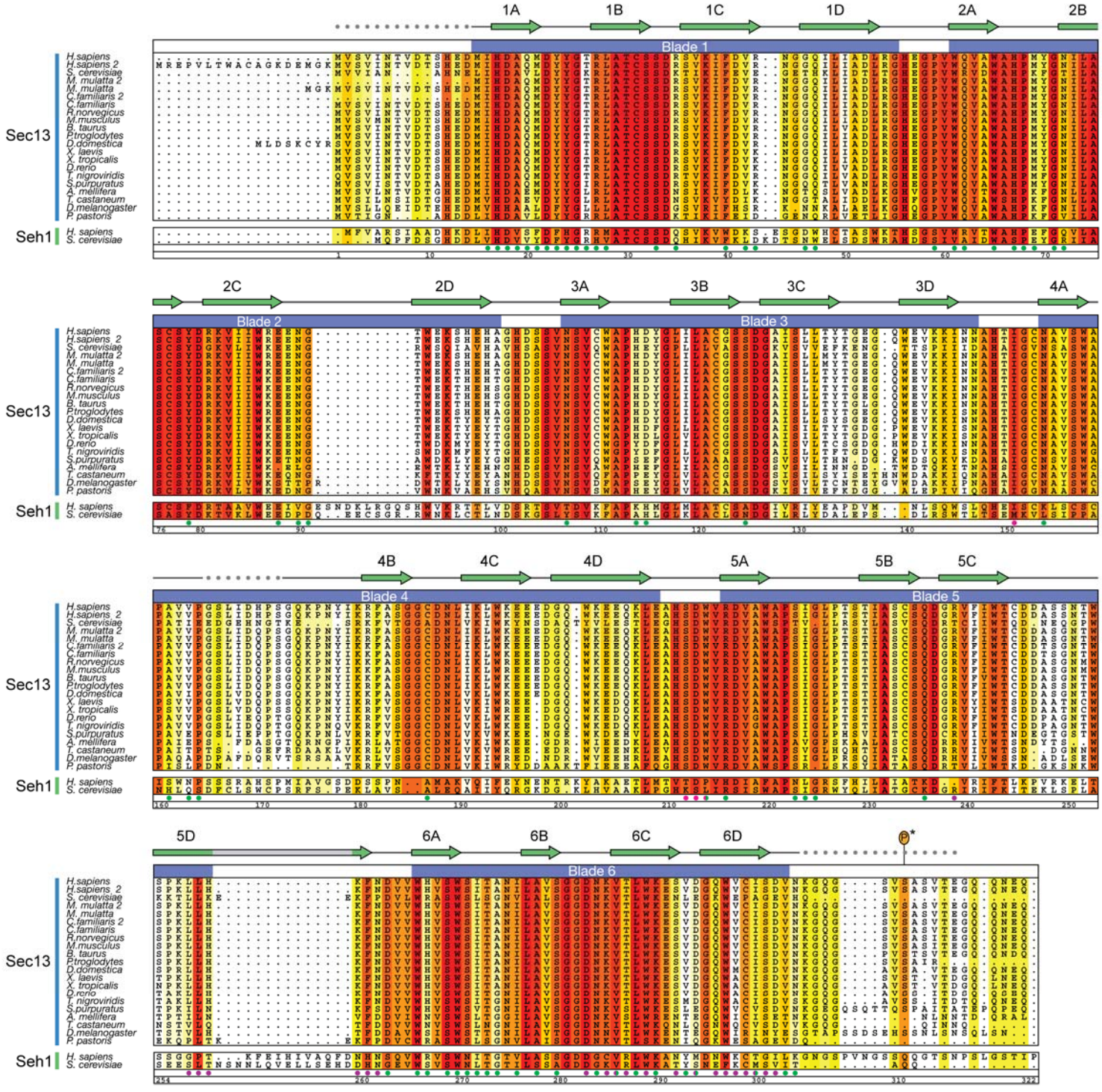

Figure S4. Multi-Species Sequence Alignment of Sec13 and Seh1 Homologs. The numbering below the alignment is relative to *H. sapiens* Sec13. The overall sequence conservation at each position is shaded in a color gradient from yellow (40% similarity) to dark red (100% identity) using the Blosum62 weighting algorithm. The secondary structure is indicated above the sequence as green arrows (β -strands), gray lines (coil regions), and gray dots (disordered residues). The participation of various residues in the formation of the Sec13-Sec13 interface (purple dots), the Sec13-Nup145C interface in the same complex (green dots), and the Sec13-Nup145C interface with an adjacent Sec13-Nup145C complex (magenta dots) is indicated below the aligned sequences. The invariant Ser311 has been identified as a putative phosphorylation site, using the Netphos and KinasePhos prediction algorithms (Blom et al., 1999; Huang et al., 2005). Seh1 has a longer C-terminal tail than Sec13 and a unique insertion in the 5D-6A inter-blade connector which is not conserved in Sec13. For clarity, these residues have been omitted from the alignment.

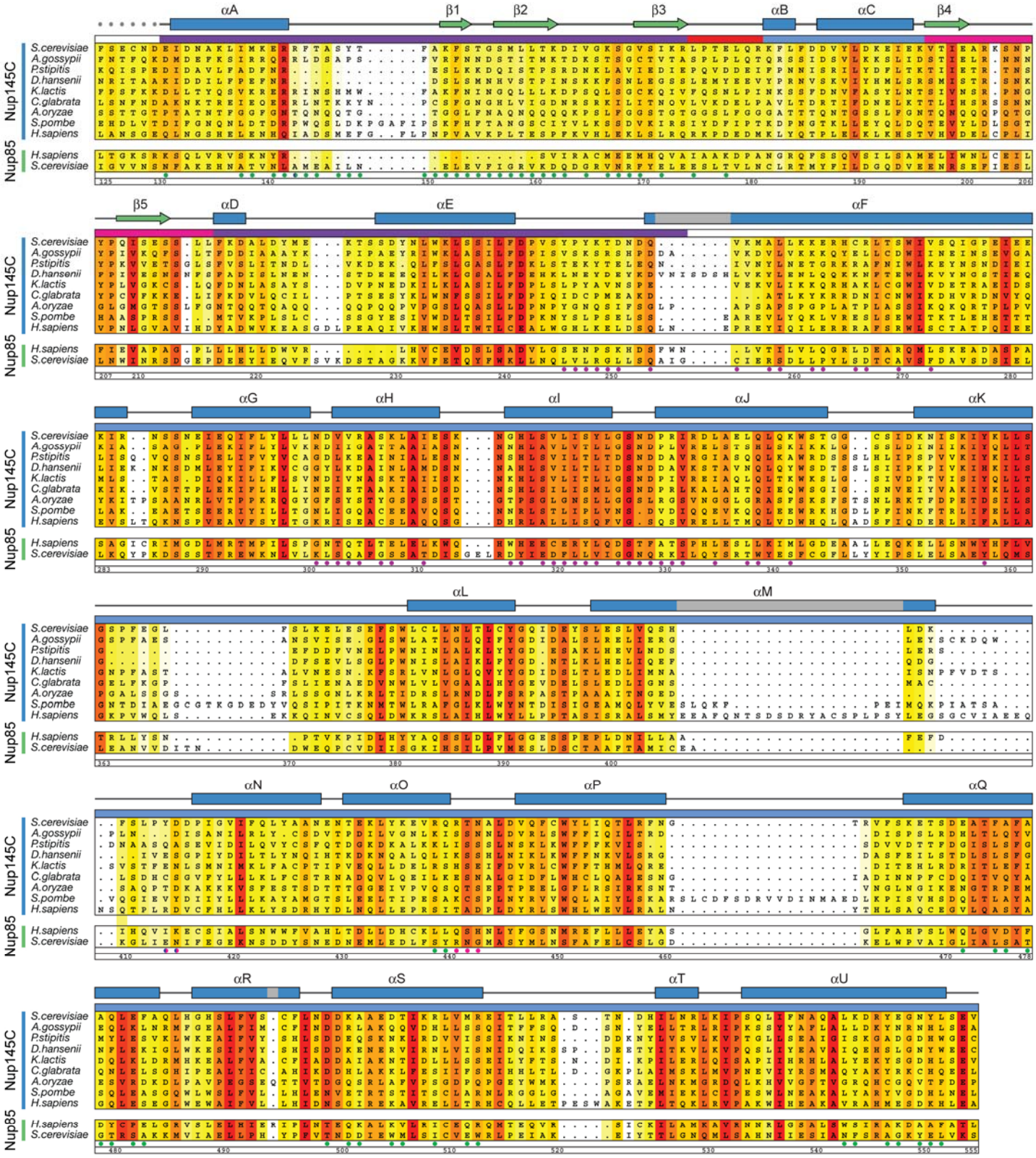

Figure S5. Multi-Species Sequence Alignment of Nup145C and Nup85 Homologs. The alignment is generated and colored, and the secondary structure elements are labeled according to Figure S4. The numbering below the alignment is relative to *S. cerevisiae* Nup145C. The participation of various residues in the Nup145C homo-dimerization interface (purple dots), the Sec13-Nup145C interface within the same complex (green dots), the Sec13-Nup145C interface to the adjacent complex (magenta dots), and the Nup145C-Nup145C center interface (blue dots) is indicated below the aligned sequences. The *H. sapiens* Nup145C homolog is termed Nup96.

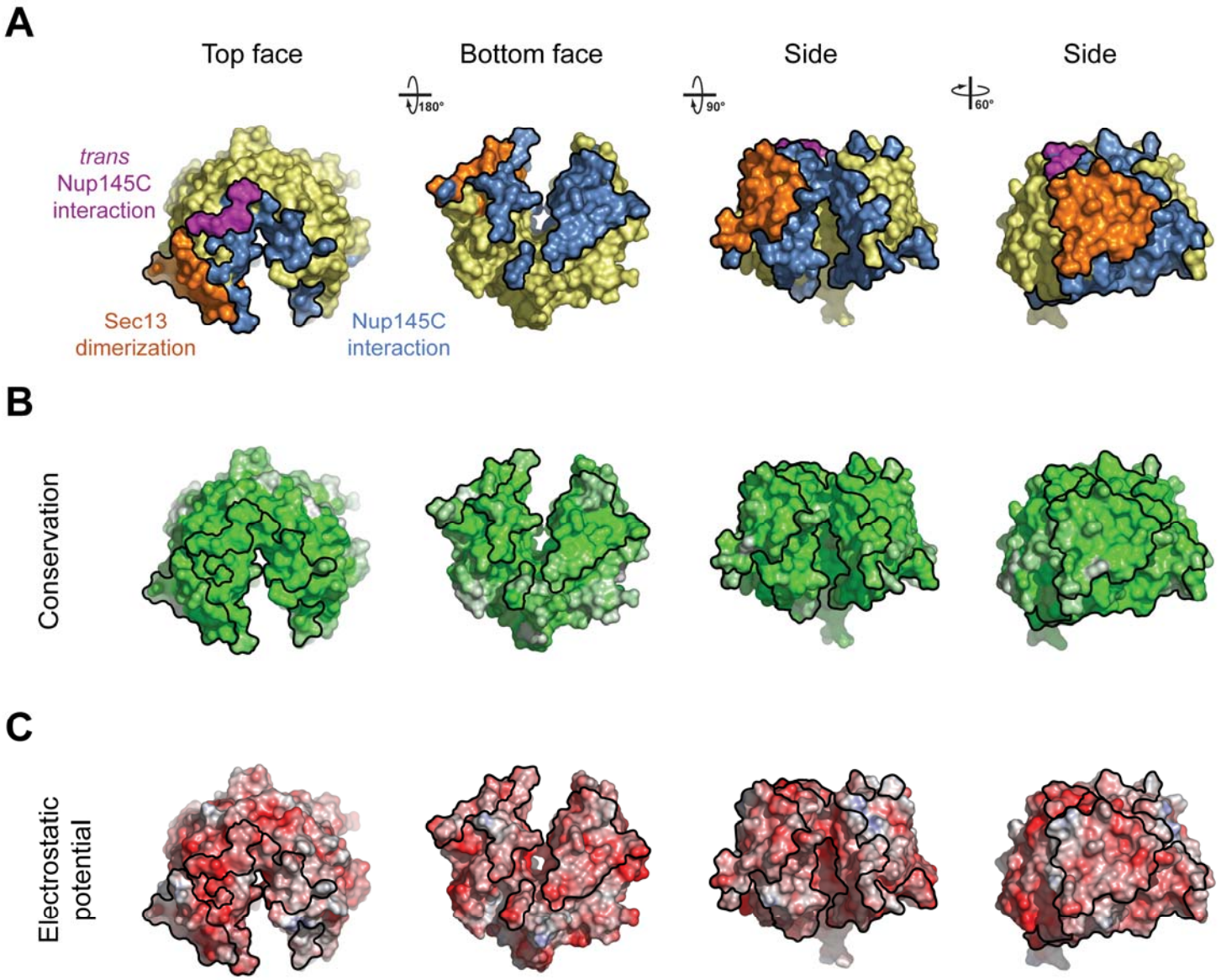

Figure S6. Surface Properties of Sec13. (**A**) Surface rendition of Sec13 (yellow), illustrating the participation of various surface patches in the interaction with Nup145C (same complex, blue; adjacent complex, purple) and the homo-dimerization with an adjacent Sec13 (orange). (**B**) Surface rendition of Sec13, colored according to sequence conservation from 40 % similarity (white) to 100 % identity (green). (**C**) Surface rendition of Sec13, colored according to the electrostatic potential, from red (-10 k_BT/e) to blue (+10 k_BT/e). The various interface borders are indicated by black lines.

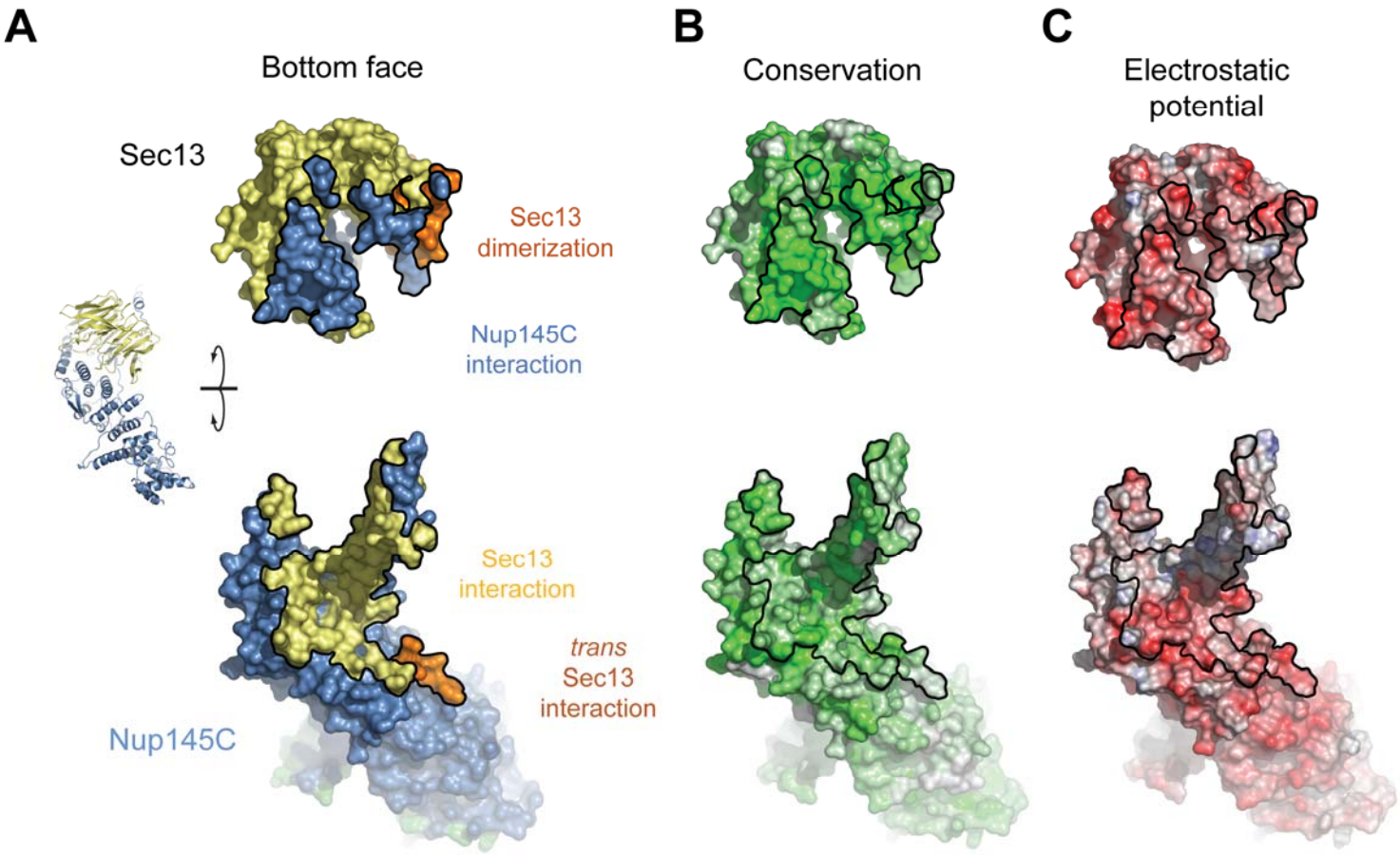

Figure S7. Surface Properties of the Sec13-Nup145C Interaction. (**A**) Surface renditions of Nup145C and Sec13 in an open book representation. The Nup145C surface (blue) is colored according to the participation of various surface patches in the interaction with Sec13 (same complex, yellow; adjacent complex, orange). The Sec13 surface is colored according to Figure S6. (**B**) Nup145C is colored according to sequence conservation, from 40 % similarity (white) to 100 % identity (green). (**C**) Surface rendition of Nup145C, colored according to the electrostatic potential, from red (-10 k_BT/e) to blue (+10 k_BT/e). The various interface borders are indicated by black lines.

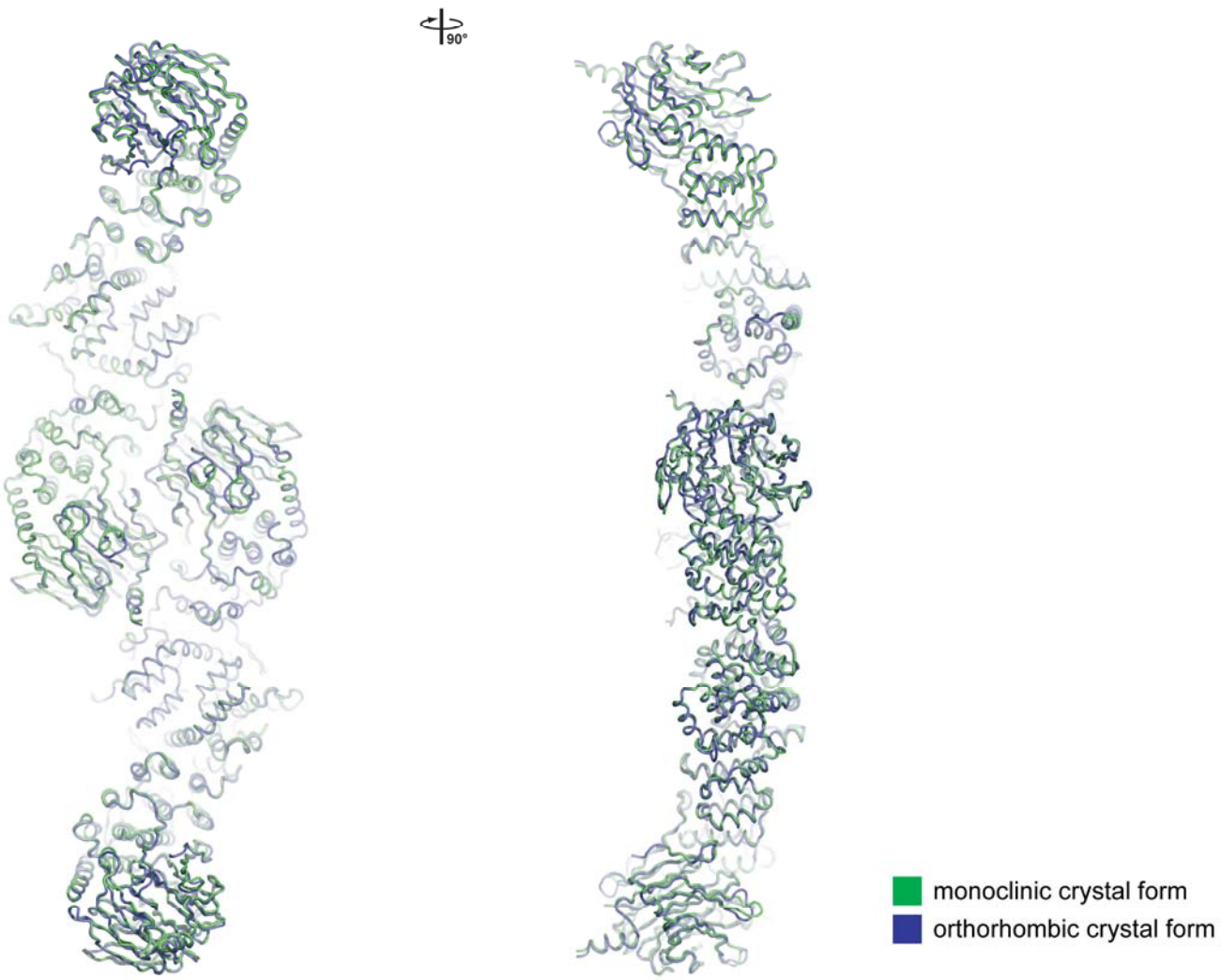

Figure S8. Comparison of the Sec13-Nup145C Structures from the Two Crystal Forms. Coil representations of the superposition of the Sec13-Nup145C hetero-octamers from the orthorhombic (green) and monoclinic (blue) crystal forms. A 90° rotated view is shown on the right.

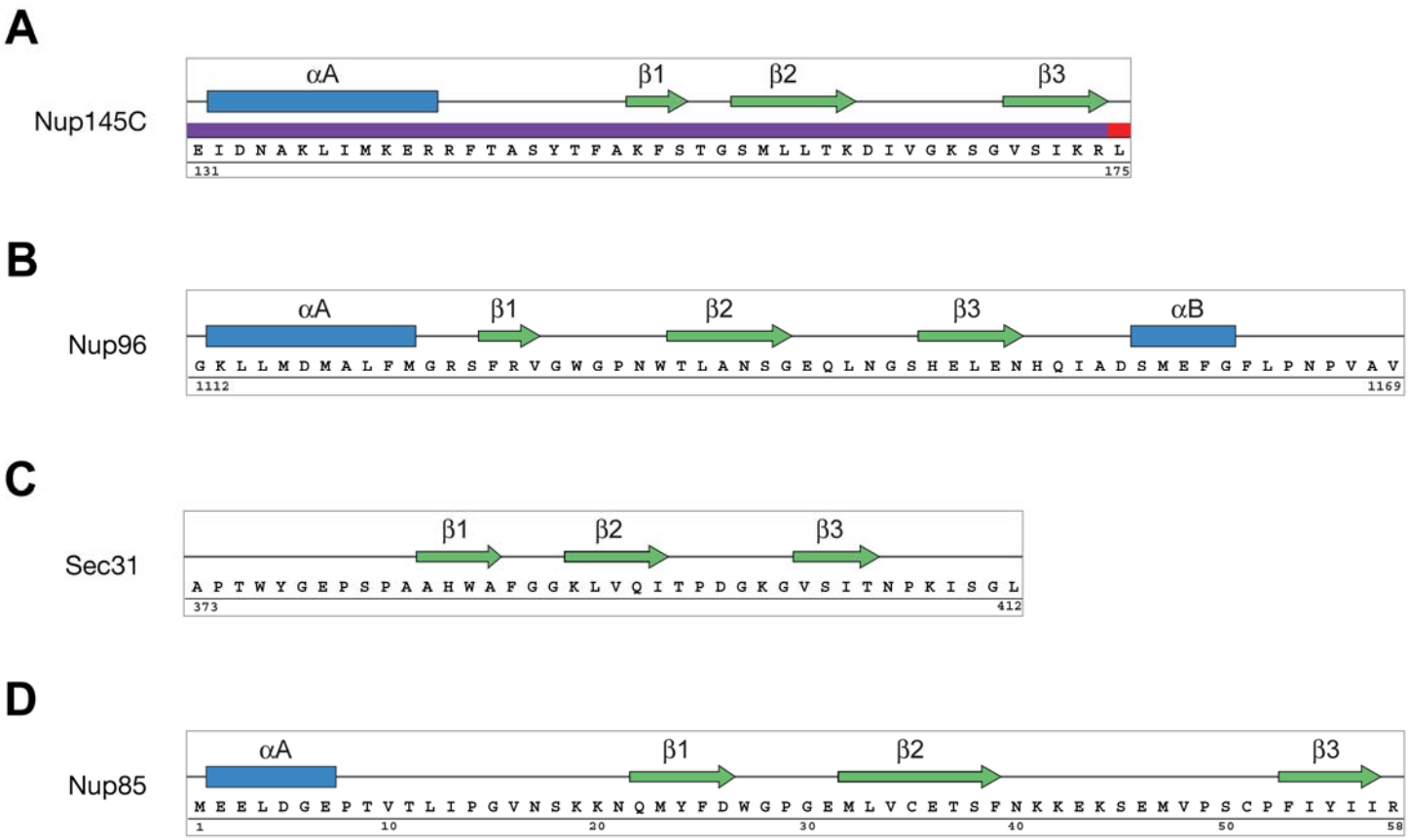

Figure S9. Topological Conservation of the DIM Secondary Structure Elements. (**A**) the Nup145C^{DIM}, (**B**) the Nup96^{DIM}, (**C**) the Sec31^{DIM}, and (**D**) the potential Nup85^{DIM}. The secondary structure prediction is indicated above the protein sequence.

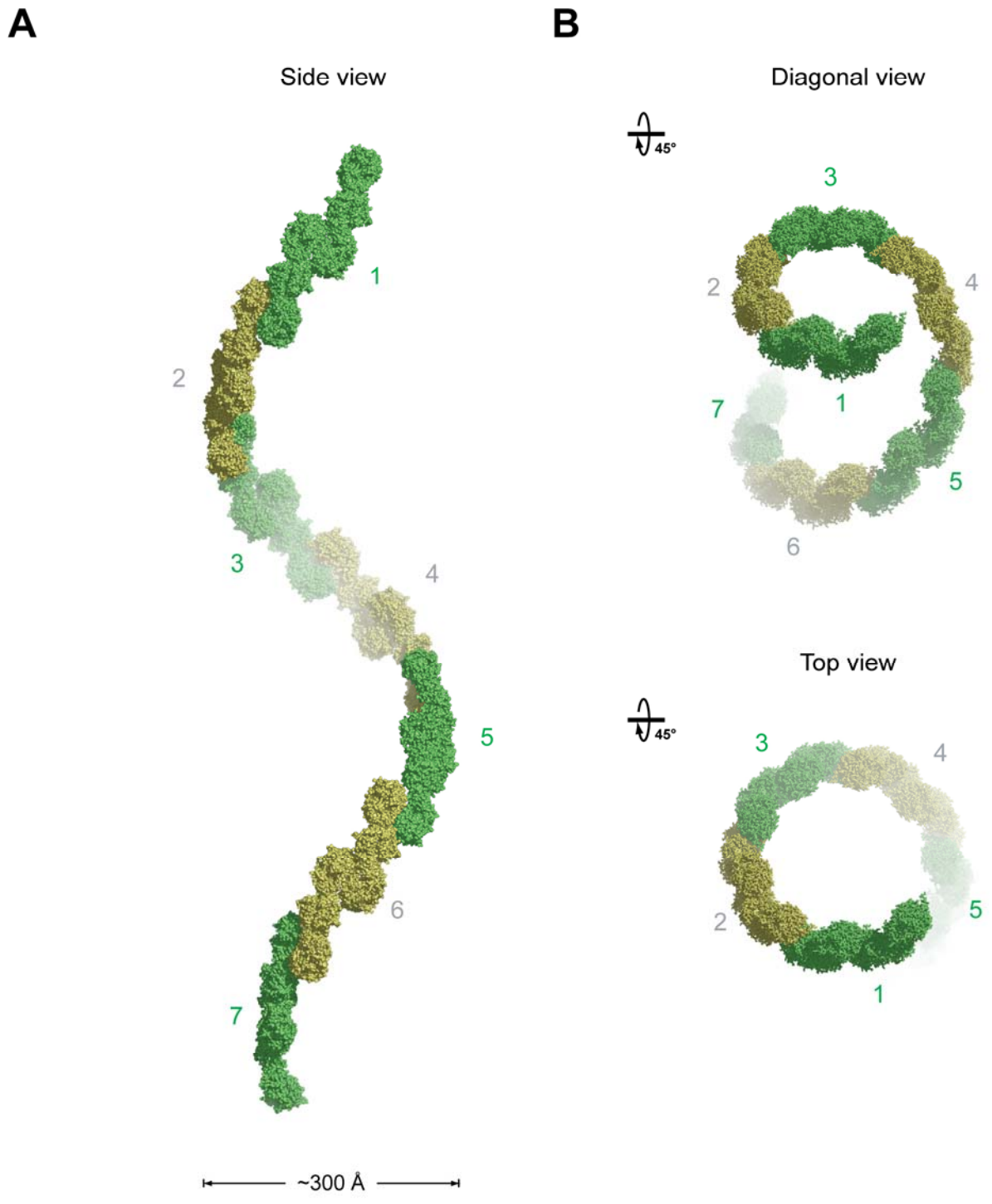

Figure S10. Model for the Higher-Order Oligomerization of the Sec13-Nup145C Hetero-Octamer. (**A**) The propagation of the oligomerization of the Sec13-Nup145C hetero-octamer does not result in the formation of a closed ring, but in a spiral with an outer diameter of ~300 Å. The Sec13-Nup145C hetero-octamers are colored in alternating yellow and green. In the assembled NPC, such an arrangement is likely irrelevant, as it is not in agreement with the oligomerization of the Seh1-Nup85 hetero-dimer (Figure 6). Note, however, that the coat cylinder cannot be extended further, because the curvature of a hetero-octamer polymer changes direction. (**B**) Diagonal and top views of the spiral. The model was generated by the sequential superpositioning of a terminal Sec13 protomer over a centrally located Sec13 protomer in order to generate an identical Sec13-Sec13 homo-dimerization interface.

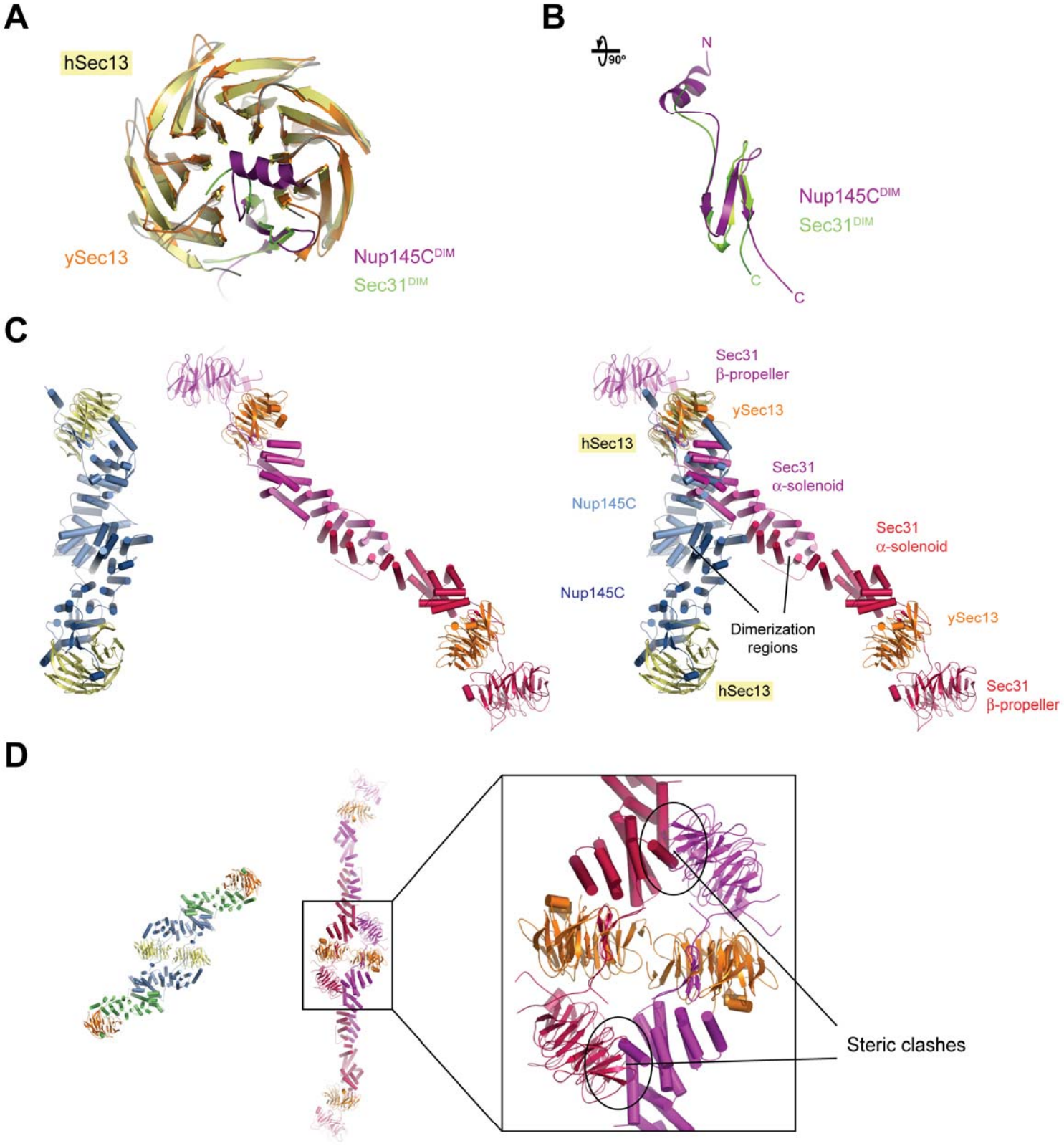

Figure S11. Structural Comparison between the Sec13-Nup145C and Sec13-Sec31 Complexes. (**A**) Superposition of the human and yeast Sec13 β-propellers, harboring the DIMs of Nup145C and Sec31. (**B**) An approximate 90° rotated view of the Nup145C and Sec31 DIMs. (**C**) Superposition of the Sec13-Nup145C and Sec13-Sec31 hetero-tetramers, based on the superposition in panel A. The Sec13-Nup145C (left) and Sec13-Sec31 (middle) hetero-tetramers are in the same orientation as in the superposition (right). (**D**) Analysis of the potential dimerization of Sec13-Sec31 hetero-tetramers into hetero-octamers via the Sec13 homo-dimerization, observed in the Sec13-Nup145C structure. Dimerization appears to be prohibited by steric clashes between Sec31 protomers.

Table S1. Crystallographic Analysis of the Orthorhombic Crystals

	Crystal 1 Native	Crystal 2 $[Ta_6Br_{12}]^{2+}$	Crystal 3 SeMet			Crystal 4 EMTS[a]	Crystal 5 K_2OsO_4			Crystal 6 K_2PtCl_4
Data collection										
Synchrotron	ALS	ALS	NSLS	NSLS	NSLS	ALS	ALS	ALS	ALS	ALS
Beamline	BL8.2.2	BL8.2.1	X29	X29	X29	BL8.2.2	BL8.2.1	BL8.2.1	BL8.2.1	BL8.2.1
Space group	$C222_1$	$C222_1$	$C222_1$	$C222_1$	$C222_1$	$C222_1$	$C222_1$	$C222_1$	$C222_1$	$C222_1$
Cell dimensions										
a, *b*, *c* (Å)	a=181.4, b=216.8, c=192.6	a=180.8, b=216.5, c=193.4	a=180.7, b=216.5, c=192.9	a=181.0, b=217.3, c=193.6	a=181.9 b=217.4, c=194.2	a=180.6, b=217.0, c=191.6	a=181.0, b=217.1, c=193.5	a=181.0, b=217.6, c=193.9	a=180.5, b=217.5, c=194.0	a=179.9, b=216.1, c=187.3
α, β, γ (°)	α=β=γ=90°	α=β=γ=90°	α=β=γ=90°	α=β=γ=90°	α=β=γ=90°	α=β=γ=90°	α=β=γ=90°	α=β=γ=90°	α=β=γ=90°	α=β=γ=90°
		Ta Peak	*Se Peak*	*Se Inflection*	*Se Remote*	*Hg Peak*	*Os Peak*	*Os Inflection*	*Os Remote*	*Pt Peak*
Wavelength	1.00000	1.25490	0.97900	0.97930	0.95000	1.00910	1.14010	1.14050	1.10700	1.07210
Resolution (Å)	20.0-3.0	50.0-4.0	30.0-3.4	30.0-3.65	30.0-3.80	50.0-3.9	50.0-3.80	50.0-3.95	50.0-4.45	50.0-4.7
R_{sym} (%)[b]	11.0 (64.6)	11.2 (55.2)	13.6 (66.4)	14.6 (72.3)	14.5 (69.2)	8.8 (60.1)	10.4 (47.7)	12.1 (65.5)	10.8 (82.8)	9.8 (79.4)
$\langle I / \sigma I \rangle$[b]	19.3 (1.7)	11.6 (2.2)	9.0 (1.7)	8.6 (1.7)	7.5 (1.8)	12.5 (2.3)	11.8 (2.9)	10.2 (2.0)	10.3 (1.7)	13.3 (1.3)
Completeness (%)[b]	97.3 (92.4)	96.7 (97.7)	99.1 (99.1)	98.8 (99.0)	95.2 (93.1)	91.8 (90.2)	99.4 (96.6)	99.4 (97.8)	99.4 (97.9)	94.8 (86.8)
Redundancy	11.2	3.1	3.3	3.2	2.8	3.2	3.7	3.7	3.7	5.0

Refinement	
Resolution (Å)	20.0-3.0
No. reflections	53,141
Test set	4,327 (8 %)
R_{work} / R_{free} (%)	24.7 / 28.9
No. atoms	22,618
R.m.s deviations	
Bond lengths (Å)	0.009
Bond angles (°)	1.6

[a]EMTS, ethylmercurithiosalicylate

[b]Highest-resolution shell is shown in parentheses.

Table S2. Crystallographic Analysis of the Monoclinic Crystals

	Crystal 1 Native	Crystal 2 $[Ta_6Br_{12}]^{2+}$			Crystal 3 K_2OsO_4		Crystal 4 EMTS[a]		Crystal 5 SeMet
Data collection									
Synchrotron	ALS	ALS	ALS	ALS	NSLS	NSLS	ALS	ALS	ALS
Beamline	BL8.2.2	BL8.2.1	BL8.2.1	BL8.2.1	X29	X29	BL8.2.1	BL8.2.1	BL8.2.2
Space group	C2	C2	C2	C2	C2	C2	C2	C2	C2
Cell dimensions									
a, *b*, *c* (Å)	a=181.8	a=180.7	a=180.8	a=181.4	a=181.1	a=181.2,	a=181.1	a=181.4,	a=181.7,
	b=216.6	b=216.9	b=217.5	b=218.0	b=218.0	b=217.3,	b=217.4	b=218.0,	b=217.2,
	c=101.0	c=101.0	c=101.5	c=101.5	c=101.2	c=100.8	c=102.1	c=102.3	c=101.7
α, β, γ (°)	α=γ=90°	α=γ=90°	α=γ=90°	α=γ=90°	α=γ=90°	α=γ=90°	α=γ=90°	α=γ=90°	α=γ=90°
	β=108.1°	β=108.2°	β=108.2°	β=108.2°	β=108.0°	β=107.9°	β=107.9°	β=107.9°	β=108.0°
		Ta Peak	*Ta Inflection*	*Br Peak*	*Os Peak*	*Os Inflection*	*Hg Peak*	*Hg Inflection*	*Se Peak*
Wavelength	1.00000	1.25480	1.25490	0.91980	1.14000	1.14040	1.00910	1.00930	0.97950
Resolution (Å)	20.0-3.15	20.0-5.0	50.0-5.0	20.0-6.5	20.0-3.75	20.0-3.75	20.0-3.60	20.0-4.0	50.0-4.0
R_{sym} (%)[b]	14.5 (74.6)	8.2 (40.9)	7.6 (42.8)	9.1 (49.8)	14.2 (83.4)	11.6 (59.2)	9.9 (90.7)	6.6 (31.1)	7.5 (31.6)
$\langle I / \sigma I \rangle$[b]	17.9 (1.9)	10.4 (1.8)	9.8 (1.8)	10.6 (1.6)	9.6 (1.4)	12.2 (1.4)	8.0 (2.1)	12.1 (2.0)	10.6 (2.2)
Completeness (%)[b]	95.7 (77.7)	96.5 (96.2)	96.8 (93.7)	98.1 (96.1)	98.7 (93.4)	97.5 (89.4)	97.3 (89.7)	97.1 (89.5)	80.2 (49.5)
Redundancy	10.8	1.9	1.9	1.9	3.5	3.4	1.8	1.7	1.8
Refinement									
Resolution (Å)	20.0-3.15								
No. reflections	55,955								
Test set	2,837 (5%)								
R_{work} / R_{free}	24.7 / 29.2								
No. atoms	22,566								
R.m.s deviations									
Bond lengths (Å)	0.009								
Bond angles (°)	1.6								

[a]EMTS, ethylmercurithiosalicylate

[b]Highest-resolution shell is shown in parentheses.

Table S3. Expression Constructs

Protein	Species	Residues	Expression vector	Restriction sites 5', 3'	N-terminal sequence overhang
Nup145C	yeast	1-711	pETDuet-1	BamHI, NotI	MGSSHHHHHHSGDP
Nup145C	yeast	125-555	pETDuet-1	BamHI, NotI	MGSSHHHHHHSGDP
Nup96	human	1112-1169	pGEX-6P1	BamHI, XhoI	GPLGGGGG
Sec13	yeast	1-297	pET24b	NdeI, XhoI	untagged
Sec13	human	1-322	pET24b	NdeI, XhoI	untagged
Sec13	human	1-316	pET24b	NdeI, XhoI	untagged
Sec13	human	1-322	pET28a-pp	NdeI, XhoI	GPHM
Seh1-Nup85	yeast yeast	1-349 (Seh1) 1-570 (Nup85)	pETDuet-1	BamHI, NotI NdeI, XhoI	MGSSHHHHHHSGDP untagged

SUPPLEMENTAL EXPERIMENTAL PROCEDURES

Protein Expression and Purification

A DNA fragment containing residues 1112-1169 of *H. sapiens* Nup96 was amplified by PCR and cloned into the BamHI and XhoI restriction sites of pGEX-6P1 (GE Heathcare). The expression of the Sec13-Nup96^{DIM} complex was carried out in the same manner as the expression of the Sec13-Nup145C complex was. However, cells were re-suspended on ice in a buffer containing 50 mM TRIS, pH 8.0, 100 mM NaCl, 5 mM DTT, bovine lung aprotinin (20 µg/ml), 2 mM PMSF, and Complete EDTA-free Protease inhibitor cocktail tablets (Roche). For purification, the cells were lysed with a cell disruptor (Avestin), and the lysate was centrifuged for 90 minutes at 40,000 g. The resulting supernatant fraction was filtered through a 0.45 µm filter (Nalgene) and loaded onto a glutathione Sepharose 4B column (GE Healthcare) that was equilibrated in buffer A (50 mM TRIS, pH 8.0, 100 mM NaCl, 5 mM DTT). The resin was first washed in buffer A, and the bound protein was eluted, using a gradient of buffer B (buffer A supplemented with 20 mM glutathione). The eluted protein fractions were pooled, extensively dialyzed against buffer A, and cleaved with GST-PreScission protease for 36 hours in order to remove the N-terminal GST-tag. Protease cleavage left an additional five residues on the N-terminus with sequence GPLGS. The sample was then loaded onto a glutathione Sepharose 4B column to remove any uncleaved protein, free GST, and GST-PreScission. After concentration, the samples were injected onto a Superdex 75 16/60 column that was equilibrated in buffer C (20 mM TRIS, pH 8.0, 100 mM NaCl, 5 mM DTT). The protein-containing fractions were pooled, concentrated to 20 mg/ml, snap-frozen in liquid nitrogen, and stored at -80°C.

SUPPLEMENTAL REFERENCES

Blom, N., Gammeltoft, S., and Brunak, S. (1999). Sequence and structure-based prediction of eukaryotic protein phosphorylation sites. J. Mol. Biol. *294*, 1351-1362.

Huang, H.D., Lee, T.Y., Tzeng, S.W. & Horng, J.T. (2005). KinasePhos: a web tool for identifying protein kinase-specific phosphorylation sites. Nucleic Acids Res. *33*, W226-229.